In vivo biased agonism at 5-HT1A receptors: characterisation by simultaneous PET/MR imaging

Benjamin Vidal, Sylvain Fieux, Jérôme Redouté, Marjorie Villien, Frédéric Bonnefoi, Didier Le Bars, Adrian Newman-Tancredi, Nicolas Costes, Luc Zimmer

In vivo biased agonism at 5-HT_{1A} receptors: characterisation by simultaneous PET/MR imaging

Benjamin Vidal[1], Sylvain Fieux[1], Jérôme Redouté[2], Marjorie Villien[2], Frédéric Bonnefoi[2], Didier Le Bars[2,3], Adrian Newman-Tancredi[4], Nicolas Costes[2] and Luc Zimmer[1,2,3]

In neuropharmacology, the recent concept of 'biased agonism' denotes the capacity of certain agonists to target-specific intracellular pathways of a given receptor in specific brain areas. In the context of serotonin pharmacotherapy, 5-HT_{1A} receptor-biased agonists could be of great interest in several neuropsychiatric disorders. The aim of this study was to determine whether biased agonists could be differentiated in terms of regional targeting by use of simultaneous functional magnetic resonance imaging (fMRI) and positron emission tomography (PET) brain imaging. We compared two 5-HT_{1A}-biased agonists, NLX-112 and NLX-101, injected at three different doses in anaesthetised cats ($n = 4$). PET imaging was acquired for 90 min after bolus administration followed by constant infusion of the 5-HT_{1A} radiotracer, [^{18}F]MPPF. Drug occupancy was evaluated after injection at 50 min and BOLD fMRI was simultaneously acquired to evaluate subsequent brain activation patterns. 5-HT_{1A} receptor occupancy was found to be dose-dependent for both agonists, but differed in magnitude and spatial distribution at equal doses with distinct BOLD patterns. Functional connectivity, as measured by BOLD signal temporal correlations between regions, was also differently modified by NLX-112 or NLX-101. Voxel-based correlation analyses between PET and fMRI suggested that NLX-112 stimulates both 5-HT_{1A} autoreceptors and post-synaptic receptors, whereas NLX-101 preferentially stimulates post-synaptic cortical receptors. In cingulate cortex, the agonists induced opposite BOLD signal changes in response to receptor occupancy. These data constitute the first simultaneous exploration of 5-HT_{1A} occupancy and its consequences in terms of brain activation, and demonstrates differential signalling by two 5-HT_{1A}-biased agonists. Combined PET/fMRI represents a powerful tool in neuropharmacology, and opens new ways to address the concept of biased agonism by translational approaches.

INTRODUCTION

Although G-protein-coupled receptors drug development has focused on conventional agonists and antagonists over the years, there is growing evidence that some agonists can preferentially stimulate intracellular signalling pathways that interact with the same receptor, a phenomenon called 'functional selectivity' or 'biased agonism'. This raises in neuropharmacology the prospect of targeting specific subpopulations of receptors expressed in different brain regions, depending on their coupling with different effectors [1]. In this regard, 5-HT_{1A} receptors are known to couple to different G-protein subtypes depending on their brain localisation [2], and several studies support the existence of 5-HT_{1A}-biased agonists able to discriminate between different populations of receptors [3]. Among these, we focus here on two structural analogues, NLX-101 (also called F15599) and NLX-112 (also known as F13640 or befiradol). Both are drug candidates for different indications—respectively for the treatment of breathing deficits in Rett syndrome [4], and L-DOPA-induced dyskinesia in Parkinson's disease [5]—and show high affinity, efficacy and specificity for the 5-HT_{1A} receptors, although in vitro studies show that they preferentially stimulate different signalling pathways [6, 7]. In vivo data in animals also suggest that NLX-101 is able to specifically target post-synaptic 5-HT_{1A} receptors at low doses, in particular cortical receptors [3], whereas NLX-112 exhibits comparable stimulation of both pre-synaptic autoreceptors in raphe, and post-synaptic receptors in various brain regions [8, 9]. However, these studies conducted in rodents used invasive and regionally limited techniques, such as electrophysiology, microdialysis or immunohistochemistry. In comparison, use of a technique such as PET/MR imaging enables in vivo exploration of biased agonism in a translationally relevant manner, by non-invasively mapping the receptor binding and functional effects of such biased drug candidates in the entire brain. In a preliminary study, we showed that fMRI is able to distinguish the effect of two different 5-HT_{1A}-biased agonists in rodent brain [10].

In this study, we used simultaneous PET-fMRI to compare for the first time the brain occupancy and activation patterns of NLX-112 and NLX-101. Each agonist was administered in cat at three different doses; 5-HT_{1A} occupancy was measured using PET imaging, while effects on neuronal activity (both in terms of activation patterns and functional connectivity), were estimated using fMRI. Different analyses were performed to combine the specific target engagement, provided by PET, and the functional properties of the drugs, provided by fMRI.

[1]Université Claude Bernard Lyon 1, Lyon Neuroscience Research Center, INSERM, CNRS, 69500 Bron, France; [2]CERMEP-Imaging Platform, 69677 Bron, France; [3]Hospices Civils de Lyon, 69002 Lyon, France and [4]Neurolixis Inc, Dana Point, CA, USA
Correspondence: Luc Zimmer (luc.zimmer@univ-lyon1.fr)

MATERIAL AND METHODS

Animals and procedures

Four male cats (Isoquimen S.L., Barcelona, Spain) weighing 3.5–5.5 kg underwent PET-MRI scans in 28 separate studies. All experiments were performed in accordance with European guidelines for care of laboratory animals (2010/63/EU). After premedication with medetomidine (30–60 µg/kg subcutaneous), anaesthesia was induced by an intramuscular injection of 30 µg/kg medetomidine and 2 mg/kg ketamine. A catheter was inserted into the cephalic vein of the forearm for radiotracer injection, and in the peritoneal cavity for 5-HT_{1A} agonist injection. After endotracheal intubation, the cat was placed in ventral decubitus in an acrylic stereotactic apparatus with ear bars. During the scan, anaesthesia was maintained by constant insufflation of 2% isoflurane and standard ventilation parameters were used (15 breaths/min; peak inspiratory pressure: 15 cm/H_2O; oxygen flow: 0.8–1 L/min). Body temperature was maintained using a heated water blanket and physiological parameters were continuously monitored.

Study design

Each cat underwent seven PET-MRI acquisitions (six pharmacological challenges with either NLX-112 or NLX-101 at 0.04, 0.08 or 0.16 mg/kg, or one saline injection) in a randomised order, with a minimum of 14 days between the scans. The 5-HT_{1A} radiotracer [^{18}F]MPPF was injected using a bolus infusion protocol. The bolus was injected at the start of the acquisition over 30 s (62 ± 19 MBq diluted in 1 mL of NaCl 0.9%) after which infusion was administered at a rate of 0.6 mL/min over 90 min, with an average K_{bol} [11] of 53 min. At 50 min, challenging drugs were injected in 1 mL of saline. In control experiments, NaCl 0.9% was administered alone. The fMRI acquisition was simultaneously performed from 30 to 70 min.

[^{18}F]MPPF radiosynthesis

[^{18}F]MPPF was synthetised using the chemical pathway previously described [12, 13] with a radiochemical yield of 25% corrected for decay. Radiochemical purity was higher than 98%. Specific activity at time of injection ranged between 100 and 320 GBq/µmol.

Data acquisition and reconstruction

Simultaneous PET and MR data were acquired on an integrated Siemens Biograph mMR scanner (Siemens Healthcare, Erlangen, Germany). PET data were acquired in list mode over 90 min starting with the bolus injection. Dynamic images were reconstructed with a fully three-dimensional (3D) ordinary Poisson OSEM reconstruction (OP-OSEM). This reconstruction used 3 iterations and 21 subsets, with point spread function (PSF) resolution consideration, and a zoom 4, yielding to a matrix of 256 × 256 and 127 slices, with voxels of 0.7 × 0.7 × 2.03 mm^3. The resulting voxel intensities were calibrated to obtain activity concentrations (e.g., in kBq/cc). Reconstructed images were slightly post filtered with a 3D Gaussian kernel (filter width 2 mm). Framing consisted in 19 frames of 5 min.

MRI acquisitions were achieved with a 4-channel flexible coil over the head, combined with a loop coil (7 cm diameter) placed on the neck. Structural MRI anatomical images were acquired with a gradient-echo T1-weighted MP-RAGE sequence within an acquisition time of 9 min. The matrix size was 128 × 128 × 88 to achieve a 0.6-mm isotropic resolution. A short echo time, TE, of 2.74 ms and long repetition time, TR, of 1330 ms were used. T1-weighting was introduced with an inversion time (TI) of 900 ms. The signal-to-noise ratio was optimised by using a flip angle of 9°. BOLD fMRI data were acquired with T2*-weighted echoplanar imaging. The matrix size was 76 × 76 and 24 slices with a voxel size of 1.2 × 1.2 × 2 mm^3 were acquired. A total of 1200 volumes were acquired during the 40-min acquisition period. The attenuation correction maps were derived from a Dixon sequence acquired during the first 30 min of scanning (160 × 160 matrix with 128 slices, with a voxel size of 1.6 × 1.6 × 2 mm^3, TR = 4 ms, TE = 1.23 ms).

PET data analyses

PET data were preprocessed using MINC Toolkit (McConnell Brain Imaging Centre, Montreal) and Turku PET Center Software. For each cat, all PET images were realigned and registered to the same space using a multi-subject MRI template, coregistered with a labelled atlas defining standard regions of interest [14]. Time-activity curves in kBq/cc were extracted from the different ROIs and bilaterally averaged. The ratio curves obtained were averaged in each condition and compared to the saline condition by a two-way ANOVA ($p < 0.05$; Graphpad Prism 6). These ratios at different time ranges were used to estimate occupancy at 5-HT_{1A} receptors by increasing doses of agonists, using the following formula:

$$\text{Occupancy}(\%) = \frac{\text{Ratio(Baseline)} - \text{Ratio(Postinjection)}}{\text{Ratio(Baseline)} - 1} \times 100$$

The time range used for baseline was between 40 and 50 min of scan. The post-injection time range was between 60 and 90 min. The occupancy values were averaged for each dose and compared to the control condition by Student's t tests ($p < 0.05$, Graphpad Prism 6). Occupancy changes compared to control were estimated by subtracting the variations occurring in the control condition.

An analysis of the PET data was also performed at the voxel level. Ratio images were generated by dividing the PET signal in each voxel by the mean signal in the cerebellum using the Turku PET Center software (*Imgratio* programme), from 40 to 50 min (baseline images) and from 60 to 90 min (post-injection images). These ratio images were smoothed using a 2 × 2 × 2 mm isotropic Gaussian filter and statistically compared using SPM12. The statistical analysis was performed at each voxel pooling the different subjects and each condition by a paired Student's t test, using the contrast [(Baseline image) – (Post-injection image)] to identify voxels where [^{18}F]MPPF binding was significantly decreased after the pharmacological challenge. Statistical significance was set at $p < 0.01$ uncorrected.

MRI data analysis

Pharmacological MRI data were analysed using SPM12. Four preprocessing steps were performed: (1) images realignment using a spatial cross-correlation algorithm to correct possible head movements during acquisition, (2) images unwarping to correct for possible magnetic field inhomogeneities, (3) spatial normalisation using the MRI template, (4) spatial smoothing using an isotropic Gaussian filter [2 × 2 × 2 mm]. For each cat and each experimental condition, a first-level statistical analysis was performed. Two time ranges were defined, a baseline time range corresponding to the first 600 scans before the pharmacological challenge (from 30 to 50 min) and a post-injection time range corresponding to the last 600 scans (from 50 to 70 min). These time ranges were introduced into a SPM block design using a general linear model (GLM) approach. For each condition (saline and different doses of agonists) of each subject, the post-injection time range was compared to the baseline to generate seven first-level parametric contrast images per subject, corresponding to the contrast [Post-injection – Baseline]$_{condition}$. The global signal was used as a regressor in the analysis to correct for confounding global effects (i.e., signal drift). Second-level analyses were carried out to determine significant variations of BOLD signal across subjects at a voxel level for each dose of agonist compared to control condition using analysis of variance (ANOVA). BOLD activation maps were generated using the contrasts [(Post-injection – Baseline)$_{Agonist}$ – (Post-injection – Baseline)$_{NaCl}$]. BOLD inhibition maps were generated using the reverse contrasts [(Post-injection – Baseline)$_{NaCl}$ – (Post-

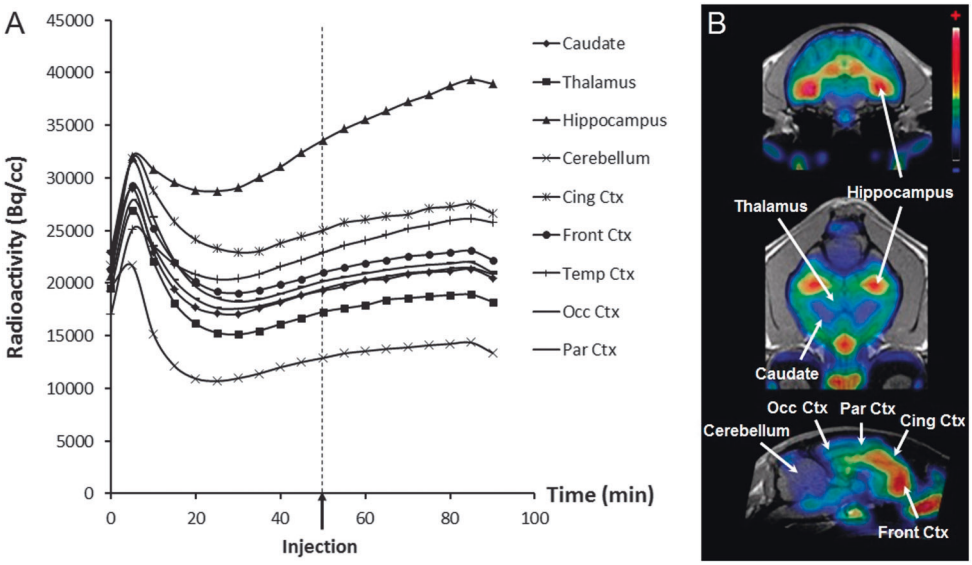

Fig. 1 Time-activity curves and cerebral distribution of [^{18}]MPPF in cat. **a** Mean time-activity curves of [^{18}F]MPPF administered in bolus + constant infusion ($n = 4$, control experiments). **b** PET images summed for 90 min on corresponding MRI, showing [^{18}F]MPPF distribution in cat brain. Cing Ctx cingulate cortex, Front Ctx frontal cortex, Occ Ctx occipital cortex, Par Ctx parietal cortex

injection − Baseline)$_{Agonist}$]. Statistical significance was set at $p < 0.05$ uncorrected. A mask was applied to include only the voxels within the brain to generate the maps.

The normalised fMRI images were also used to evaluate the functional connectivity between regions. The cat brain atlas [14] was used to extract the BOLD signal on all images in the different regions of interest. The signal was also extracted in the dorsal raphe nucleus after delineation on the MRI template according to the results of the voxel-based PET analysis. For each scan, the signal was expressed in percentage compared to the mean baseline (corresponding to the 600 first images). Temporal correlations between the different regions were then measured for each fMRI acquisition using the Pearson correlation coefficient, which was calculated for every pairs of regions during the whole time interval of 40 min. For each scan, the correlation matrix displaying the correlation coefficients for every pairs of regions was generated using Graphpad Prism 7. For each condition, the matrices were averaged to obtain mean correlation matrices.

PET/fMRI correlations

A correlation analysis was performed between 5-HT$_{1A}$ occupancy (PET data) and BOLD signal variations (fMRI data) at each voxel using the toolbox biological parametric mapping (BPM). This toolbox is designed to work jointly with SPM5 and is based on a voxel-wise use of the GLM [15]. The previous PET ratio images were used to generate an estimation of 5-HT$_{1A}$ occupancy at the voxel level for each acquisition by subtracting the post-injection image to the baseline image. The first-level analysis contrast images were used for the fMRI data. For each agonist, the correlation between 5-HT$_{1A}$ occupancy and BOLD signal changes was measured at each voxel across the different doses (three doses and saline), for all subjects. The map obtained was imported using SPM5 to visualise significant correlations between PET and fMRI at each voxel (statistical significance set at $p < 0.05$). *P* values are calculated from the correlation field using an approximation formula applied by BPM, provided that the image smoothness is the same in the two imaging modalities. A mask was applied to include only the voxels within the brain to generate the maps (cerebellum not included as this whole region was used as reference to generate the ratios images in PET).

RESULTS

PET data

[^{18}F]MPPF binding was high in hippocampus, cingulate cortex and temporal cortex (Fig. 1a), in agreement with previous studies in the cat [12, 13, 16]. Time-activity curves (TACs) showed high initial radioactivity uptake in the whole brain after the bolus injection, followed by elimination of the tracer, rapidly compensated by the constant infusion. In most experiments, TACs gradually and linearly increased. However, after 30 min, the ratios of radiotracer concentration in the regions of interest (ROIs) to the cerebellum ($C_{ROIs}/C_{Cerebellum}$, which will be referred to as 'binding ratios', BR), computed in 5-min intervals, reached constant values in control acquisitions, except in the hippocampus (Fig. 1b).

PET region of interest analysis

After its injection at 50 min, NLX-112 inhibited [^{18}F]MPPF binding in various brain regions compared to the control experiments (Fig. 2a). In 5-HT$_{1A}$-rich regions, such as the cingulate cortex and the hippocampus, BR were dose-dependently reduced by NLX-112, with a visible trend at 0.04 mg/kg, a more pronounced effect at 0.08 mg/kg and a maximal decrease at 0.16 mg/kg. In the caudate nuclei and the thalamus, a decrease was visualised at 0.16 mg/kg. Effects of NLX-112 on the BR were highly significant in the frontal cortex (two-way ANOVA; treatment, $F(3,132) = 42.86$, $p < 0.0001$; time, $F(10,132) = 26.44$, $p < 0.0001$; interaction, $F(30,132) = 3.75$, $p < 0.0001$) and the cingulate cortex (treatment, $F(3,132) = 30.84$, $p < 0.0001$; time, $F(10,132) = 17.60$, $p < 0.0001$; interaction, $F(30,132) = 2.40$, $p = 0.0004$), but even more pronounced in other cortical areas like the occipital cortex (treatment, $F(3,132) = 55.67$, $p < 0.0001$; time, $F(10,132) = 22.75$, $p < 0.0001$; interaction, $F(30,132) = 4.63$, $p < 0.0001$) and the parietal cortex (treatment, $F(3,132) = 47.79$, $p < 0.0001$; time, $F(10,132) = 35.43$, $p < 0.0001$; interaction, $F(30,132) = 4.00$, $p < 0.0001$). In the most affected cortical regions, post hoc tests (Bonferroni corrected) showed a significant decrease of [^{18}F]MPPF binding induced by NLX-112 compared to saline injection at 90 min only for the lowest doses, and from 65 to 90 min at 0.16 mg/kg.

NLX-101 inhibited [^{18}F]MPPF BR in several brain regions but not as clearly and proportionally as NLX-112 (Fig. 2b). In cortical regions and the hippocampus, a slight increase was observed at 0.04 mg/kg compared to control. At 0.08 mg/kg, curves were

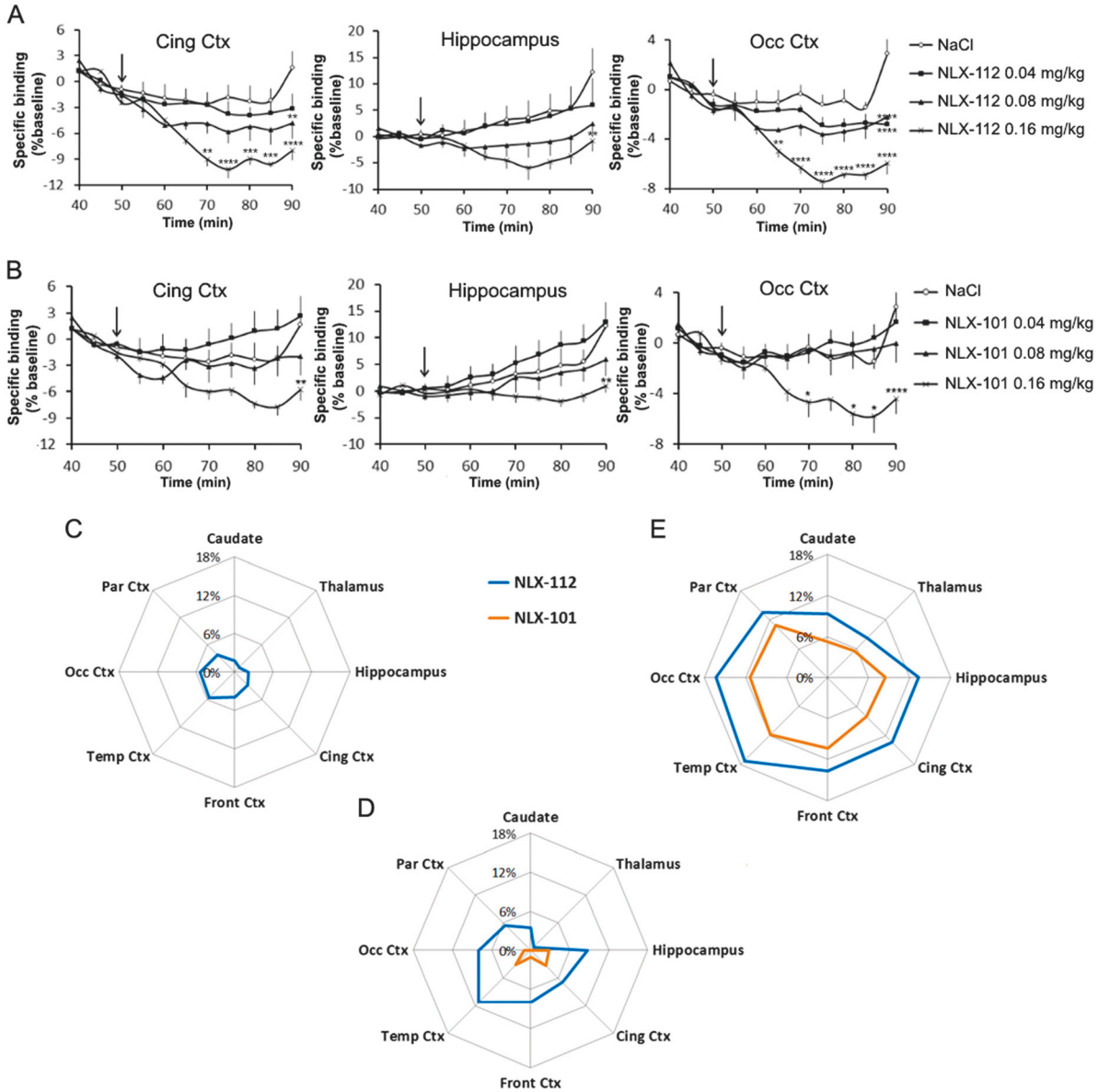

Fig. 2 Results of PET data analysis in different regions of interest. Top: [^{18}F]MPPF-specific binding (ratios to cerebellum); pharmacological challenge with NLX-112 (**a**) or NLX-101 (**b**) at $t = 50$ min (arrow). Results are expressed in percentage compared to baseline between 40 and 50 min ($n = 4$, ±standard deviation). $^{**}p < 0.01$; $^{***}p < 0.001$; $^{****}p < 0.0001$ (Bonferroni's post hoc test compared to control condition). Down: 5-HT$_{1A}$ occupancy by NLX-101 and NLX-112 at increasing doses. Results are expressed in percentage of occupancy ($n = 4$). **c** Doses of 0.04 mg/kg; **d** Doses of 0.08 mg/kg; **e** Doses of 0.16 mg/kg. Cing Ctx cingulate cortex, Front Ctx frontal cortex, Occ Ctx occipital cortex, Par Ctx parietal cortex, Temp temporal cortex

close to the control condition. A decrease was observed in these regions at 0.16 mg/kg, and also in the caudate and the thalamus to a lesser extent. Effects of NLX-101 were mostly significant in the parietal cortex (treatment, $F(3,132) = 45.94$, $p < 0.0001$; time, $F(10,132) = 14.50$, $p < 0.0001$; interaction, $F(30,132) = 3.56$, $p < 0.0001$), the frontal cortex (treatment, $F(3,132) = 30.97$, $p < 0.0001$; time, $F(10,132) = 5.95$, $p < 0.0001$; interaction, $F(30,132) = 2.62$, $p < 0.0001$), the occipital cortex (treatment, $F(3,132) = 21.28$, $p < 0.0001$; time, $F(10,132) = 4.09$, $p < 0.0001$; interaction, $F(30,132) = 2.03$, $p = 0.0035$) and the cingulate cortex (treatment, $F(3,132) = 17.26$, $p < 0.0001$; time, $F(10,132) = 4.64$, $p < 0.0001$; interaction, $F(30,132) = 1.56$, $p = 0.0469$). Bonferroni's post hoc tests compared to saline injection were not significant at 0.04 and 0.08 mg/kg, and were significant at 0.16 mg/kg from 70 to 90 min in the parietal, occipital and frontal cortices.

The mean BR during baseline (40–50 min) and post injection (60–90 min) were used to compute 5-HT$_{1A}$ occupancy by the different doses of NLX-112 and NLX-101 (Fig. 2c–e). At 0.04 mg/kg of NLX-112, 5-HT$_{1A}$ occupancy varied from 4 to 8% and was not significantly higher than control in any ROI (Student's t test, $p > 0.05$). At 0.08 mg/kg of NLX-112, 5-HT$_{1A}$ occupancy was significant in frontal and occipital cortices (about 8%), and almost significant in the hippocampus and the parietal cortex (5% with $p = 0.0666$, and 13% with $p = 0.0606$, respectively). A dose of 0.16 mg/kg of NLX-112 occupied significantly 5-HT$_{1A}$ receptors in all regions of interest apart from the thalamus, from 9 to 17%. At 0.04 mg/kg, NLX-101 occupancy was zero in all regions of interest. At 0.08 mg/kg, the occupancy was close to zero (maximum of 3%) and not significant. At 0.16 mg/kg, 5-HT$_{1A}$ occupancy by NLX-101 was significant in frontal, occipital and parietal cortices and in the caudate nucleus, and varied between 5 and 11%.

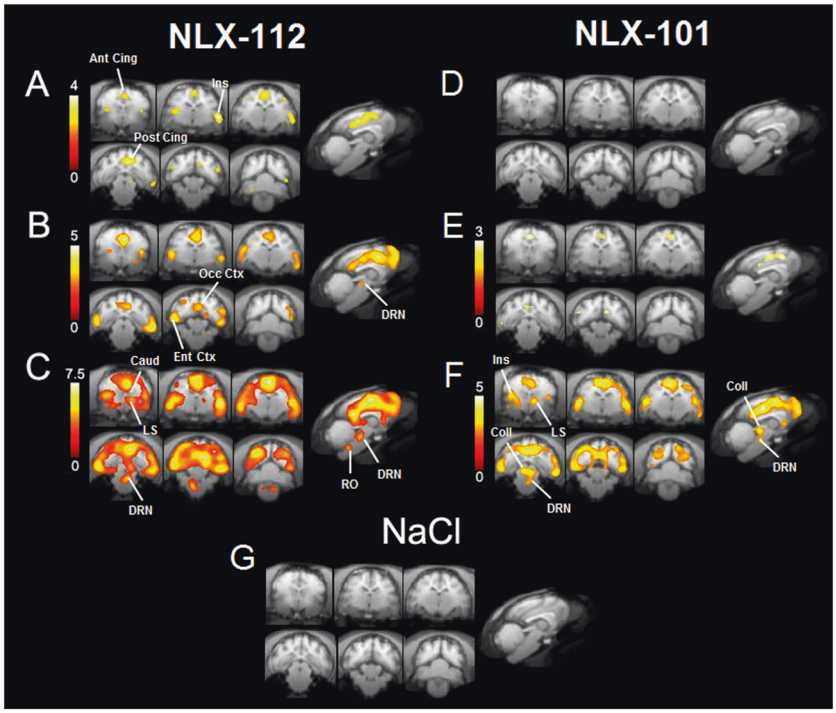

Fig. 3 Areas of significant decrease of [^{18}F]MPPF binding following injection of NLX-112 at 0.04 mg/kg (**a**), 0.08 mg/kg (**b**) and 0.16 mg/kg (**c**) or NLX-101 at 0.04 mg/kg (**d**), 0.08 mg/kg (**e**) and 0.16 mg/kg (**f**) in cat brain ($n = 4$). Voxel-to-voxel statistical comparison between [^{18}F]MPPF-specific binding from 60 to 90 min and [^{18}F]MPPF-specific binding from 40 to 50 min (Student's t test, $p < 0.01$). T scores in left scales. No voxel appeared significantly different between post injection and baseline following the injection of NaCl 0.9% (**g**). Ant Cing anterior cingulate cortex, Caud caudate nucleus, Coll colliculus, DRN dorsal raphe nucleus, Ent Ctx entorhinal cortex, Ins insula, LS lateral septum, Occ Ctx occipital cortex, Post Cing posterior cingulate cortex, RO raphe obscurus

PET voxel analysis

[^{18}F]MPPF-binding ratio between baseline and post-injection time ranges was compared at the voxel level with SPM, for each doses of 5-HT$_{1A}$ agonists, and for saline. This analysis enabled to map the occupancy of 5-HT$_{1A}$ receptors by agonists at the voxel level. The statistical analysis did not show any significant change of [^{18}F]MPPF binding occurring after saline injection (Fig. 3g).

A dose of 0.04 mg/kg of NLX-112 induced a significant decrease of the specific binding in the anterior and posterior cingulate cortices, in the insula and the entorhinal cortex (Fig. 3a). At 0.08 mg/kg of NLX-112, a decrease of radiotracer binding was found in the cingulate, insular, entorhinal and occipital cortices with a more expanded pattern. A slight decrease was also found in few voxels located in the dorsal raphe nucleus (see sagittal view of Fig. 3b). At 0.16 mg/kg (Fig. 3c), NLX-112 strongly decreased [^{18}F]MPPF binding in multiple cortical areas. Few significant voxels were also observed in the amygdala, lateral septum and caudate in the rostral part of the brain. In the caudal part, significant clusters were found in the dorsal raphe nucleus and the raphe obscurus (see sagittal view of Fig. 3c).

For NLX-101, no occupancy was detected in any voxel at 0.04 mg/kg, similarly to saline injection (Fig. 3d). At 0.08 mg/kg, some significant voxels were found in the cingulate cortex (Fig. 3e). At 0.16 mg/kg, the tracer binding was strongly decreased in cortical areas, similarly to NLX-112 (Fig. 3f). Few significant voxels were also found in the lateral septum, the colliculi and the dorsal raphe (to a lesser extent than NLX-112).

fMRI voxel analysis

In parallel to 5-HT$_{1A}$ occupancy, hemodynamic changes elicited by NLX-112 and NLX-101 were measured using fMRI. At low dose, NLX-112 induced BOLD signal inhibitions in the cingulate cortex, the amygdala, and the temporal and occipital cortices (Fig. 4a). At 0.08 mg/kg, significant BOLD decreases were found in the amygdala and the ventral hippocampus (Fig. 4b). BOLD activations were observed in the frontal cortex (see sagittal view of Fig. 4b) and the cerebellum, comparably to the lower dose, but also in the dorsal raphe nucleus. At 0.16 mg/kg, NLX-112 induced wider BOLD changes, with inhibitions mainly found in the cingulate, temporal and occipital cortices, the insula and the amygdala (Fig. 4c). BOLD activations were found in the frontal cortex, the dorsal raphe nucleus and the cerebellum, and also in the right temporal cortex.

At the lowest dose, NLX-101 induced widespread significant modifications of BOLD signal (Fig. 4d). Inhibitions were found in the amygdala and in the motor and occipital cortices. Activated areas were smaller and located in the lateral septum, the median raphe, the cerebellum, the frontal cortex and the right insula. At 0.08 and 0.16 mg/kg, fewer BOLD changes were observed (Fig. 4e, f). Inhibitions were found in few voxels of the ventral hippocampus. Activations were mainly located in the cerebellum and the frontal cortex.

fMRI functional connectivity analysis

In the control condition (saline injection), the highest correlations were found between cortical regions (Fig. 5a, b), especially between the frontal, cingulate and parietal cortices (r from 0.93 to 0.97). There were also high correlations ($r > 0.7$) between the occipital cortex, the thalamus and the cerebellum, and between the caudate nuclei and the cingulate, frontal and parietal cortices (Fig. 5a, b). At 0.04 mg/kg of NLX-112 (Fig. 5c, e), the correlation coefficients were higher than 0.7 for every pair of cortical regions (r from 0.80 to 0.97) except between the frontal and the temporal cortex ($r = 0.68$). Effects in the hippocampus and the thalamus were also highly correlated with each other ($r = 0.87$) and with the whole cortex (r from 0.75 to 0.89).

At the same dose of NLX-101, a temporal correlation between cortical regions was also observed (r from 0.73 to 0.94), with the exception of the temporal cortex (Fig. 5d, e). The cerebellum was

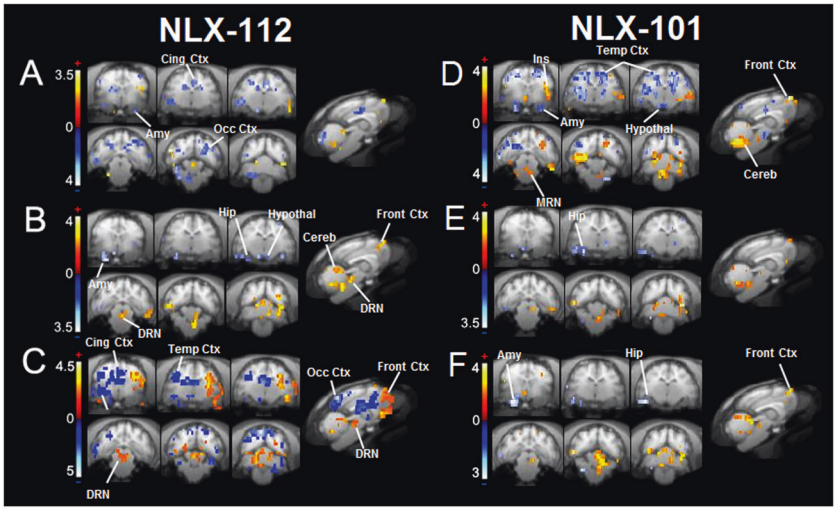

Fig. 4 Areas of significant modifications of BOLD signal following injection of NLX-112 at 0.04 mg/kg (**a**), 0.08 mg/kg (**b**) and 0.16 mg/kg (**c**), or NLX-101 at 0.04 mg/kg (**d**), 0.08 mg/kg (**e**) and 0.16 mg/kg (**f**) in cat brain ($n = 4$). Voxel-to-voxel statistical comparisons between NLX-112 and NLX-101 scans versus control scans (ANOVA, $p < 0.05$). *T* scores in left scales; significant BOLD activations in yellow to red, significant BOLD inhibitions in blue. Amy amygdala, Cereb cerebellum, Cing Ctx cingulate cortex, DRN dorsal raphe nucleus, Front Ctx frontal cortex, Hip hippocampus, Hyp hypothalamus, Ins insula, MRN median raphe nucleus, Occ Ctx occipital cortex, Temp Ctx temporal cortex

also highly correlated with the cortex (apart from the temporal part).

At the intermediate dose of the agonists (0.08 mg/kg i.p.), correlation matrices of NLX-101 and NLX-112 were similar (Fig. 5f–h). There were high correlation coefficients ($r > 0.83$) between all regions of interest, excluding the thalamus. For NLX-112, there was also a high correlation between the dorsal raphe nucleus and the other regions (r from 0.71 to 0.80), contrary to NLX-101 ($r < 0.42$).

At 0.16 mg/kg of NLX-101, the high correlations between the cortex, hippocampus and cerebellum were maintained (r from 0.76 to 0.96). At the same dose of NLX-112, the correlation matrix was strongly changed compared to the previous dose (Fig. 5i). The highest correlations were found between the cingulate cortex and parietal cortex ($r = 0.96$) or occipital cortex ($r = 0.80$), the frontal cortex and temporal cortex ($r = 0.90$), and the occipital cortex and parietal cortex ($r = 0.84$). Other strong correlations ($r > 0.7$) were found between the thalamus and cortical regions (without the occipital cortex), the hippocampus and cingulate cortex ($r = 0.71$) or parietal cortex ($r = 0.75$), the parietal cortex and temporal cortex ($r = 0.76$), the occipital cortex and caudate ($r = 0.74$) or cerebellum ($r = 0.74$).

PET/fMRI correlations

This approach was used to determine for each voxel if occupancy of 5-HT_{1A} receptors by agonists was correlated with positive or negative hemodynamic changes. A PET/fMRI correlation map was generated for each agonist (Fig. 6). For NLX-112, negative correlations (decreases of BOLD signal related to increases of 5-HT_{1A} occupancy) were observed in the cingulate cortex, the lateral septum, the insula, the amygdala and the occipital cortex, and also in parts of the brainstem. Positive correlations (increases of BOLD related to increases of 5-HT_{1A} occupancy) were found in the right motor cortex and, notably, in the dorsal raphe. The NLX-101 correlation map was very different, with few negative correlations restricted to the brainstem and the occipital cortex. A strong positive correlation was found in the cingulate cortex.

DISCUSSION

In this multimodal imaging study, complementary information provided by PET and fMRI was used to explore in vivo the concept of biased agonism at 5-HT_{1A} receptors. Although fMRI offers the opportunity to map changes in cerebral activity occurring after administration of drugs, it lacks mechanistic specificity as it provides no information on the receptors primarily targeted [17]. On the contrary, PET is able to quantify receptor occupancy by drugs at pharmacological doses, based on the competition with a specific radiotracer [18], without functional information. Simultaneous measurement of BOLD signal and receptor occupancy is therefore an attractive strategy to generate novel and critical information on the mechanism of action of CNS drugs and their neurovascular coupling [19–23]. In the context of biased agonism, it is theoretically possible to show that different agonists can stimulate different transduction pathways while binding on the same receptors, or even that they induce hemodynamic changes in different regions due to the stimulation of different subpopulations of receptors. Indeed, several 5-HT_{1A} agonists have been previously shown to stimulate different intracellular pathways (see ref. [3] for a review), or sometimes to act either as an agonist or an antagonist depending on the biochemical background tested (for instance, [^{11}C]CUMI-101 which was both reported as an agonist or an antagonist—see refs. [24, 25]). As 5-HT_{1A} receptors are coupled to different G proteins depending on their localisation [2], using biased 5-HT_{1A} ligands would enable targeting of specific subpopulations of receptors depending on their preferred transduction pathway. To date, only a few imaging studies have explored the regional selectivity of 5-HT_{1A} ligands in vivo, in terms of receptor occupancy using PET [26, 27] or hemodynamic effects using fMRI [10], but never using both modalities simultaneously.

In the present study, we focused on two structural analogues, NLX-112 and NLX-101. These full 5-HT_{1A} agonists display similar affinities at 5-HT_{1A} receptors—Ki = 2.2 nM for NLX-101; Ki = 0.85 nM for NLX-112 [28]—with a high target specificity [6, 29] but with marked differences in terms of their in vitro intracellular signalling pathways [6, 7]. In vivo, the main reported difference between NLX-112 and NLX-101 concerns the capacity of NLX-101 to interact preferentially with post-synaptic 5-HT_{1A} receptors, especially cortical receptors, with little capacity to stimulate the pre-synaptic 5-HT_{1A} autoreceptors located in raphe nuclei (for a review, see ref. [3]). On the contrary, NLX-112 interacts with both pre- and post-synaptic receptors [8, 30].

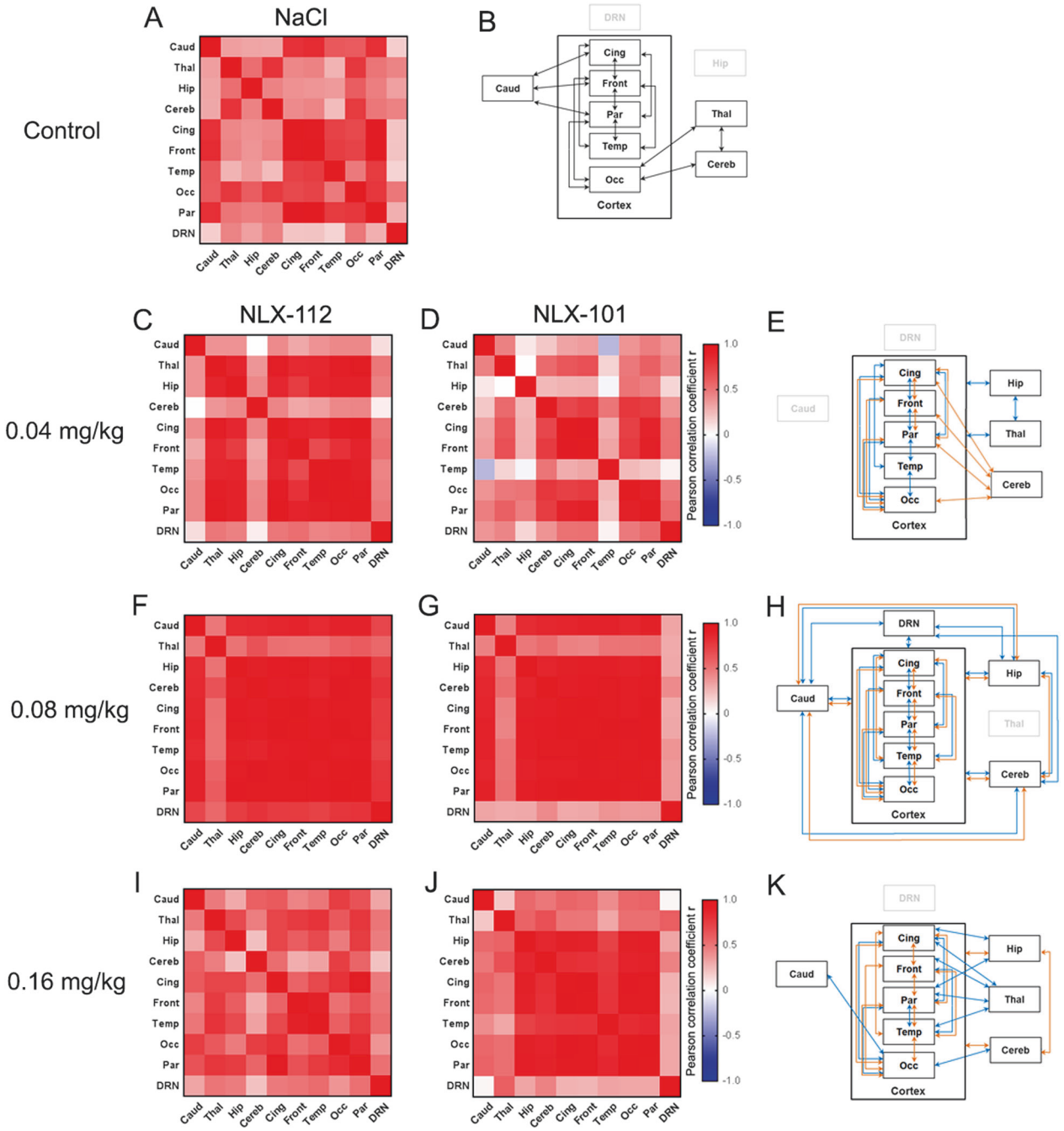

Fig. 5 Functional connectivity analysis following injection of saline (**a**, **b**), NLX-112 at 0.04 mg/kg (**c**, **e**), 0.08 mg/kg, (**f**, **h**) and 0.16 mg/kg (**i**, **k**), or NLX-101 at 0.04 mg/kg (**d**, **e**), 0.08 mg/kg (**g**, **h**) and 0.16 mg/kg (**j**, **k**) in cat brain ($n = 4$). Correlation matrices are shown in **a** (saline), **c**, **d** (doses of 0.04 mg/kg), **f**, **g** (doses of 0.08 mg/kg), **i**, **j** (doses of 0.16 mg/kg), with colour bar indicating values of Pearson correlation coefficient *r*. Graphical representations for each dose are shown in (**b**) (saline), **e** (doses of 0.04 mg/kg), **h** (doses of 0.08 mg/kg) and **k** (doses of 0.16 mg/kg). Each rectangle corresponds to a region of interest; to simplify the data interpretation, each arrow between two regions corresponds to a value of $r > 0.7$. Black arrows correspond to the functional connectivity in the saline condition; blue arrows represent the functional connectivity for NLX-112; orange arrows represent the functional connectivity for NLX-101. Cortical regions are grouped in a global region called cortex, in order to facilitate visualisation when a region is functionally connected with all cortical regions

5-HT_{1A} occupancy

The analysis of PET data at the regional level showed that occupancy of 5-HT_{1A} receptors by NLX-112 increases proportionally from 0.04 to 0.16 mg/kg. On the contrary, occupancy was clearly detected only at 0.16 mg/kg for NLX-101, with almost no decrease of [^{18}F]MPPF-specific binding at 0.08 mg/kg and a slight paradoxical increase at 0.04 mg/kg. This was not statistically significant, and is probably not due to a decrease of endogenous serotonin release, as [^{18}F]MPPF is only sensitive to massive changes in extracellular serotonin concentration [31, 32]. In any case, two main conclusions can be driven based on this analysis. First, NLX-101 occupancy of 5-HT_{1A} receptors is limited compared to NLX-112 at equal doses, which could be explained by its slightly lower affinity for 5-HT_{1A} receptors (2.2 nM versus 0.85 nM), and by its reported biased properties. Second, the occupancy does not increase linearly with the agonist dose across the different regions,

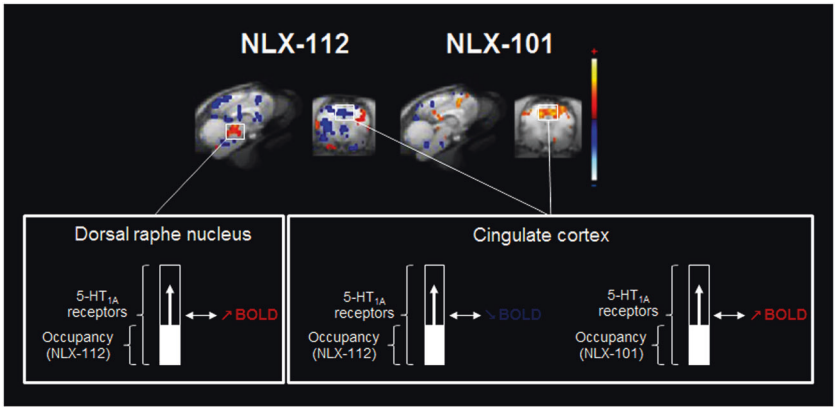

Fig. 6 PET-fMRI correlation maps corresponding to significant correlations between 5-HT_{1A} occupancy and BOLD signal change for each 5-HT_{1A} agonist. Positive correlations in red, negative correlations in blue ($p < 0.05$)

and at equal doses the occupancy spatial profile can be very different between two agonists. This result suggests that biased agonism and targeting of 5-HT_{1A} receptors in specific regions is very dependent on the dose.

These observations were confirmed by the voxel-based analysis. 5-HT_{1A} receptor occupancy by NLX-112 was mostly found in multiple regions expressing post-synaptic receptors, at all three doses. This approach also enabled to visualise occupancy of autoreceptors in the dorsal raphe nucleus at 0.08 and 0.16 mg/kg of NLX-112. In contrast, at 0.08 mg/kg, NLX-101 targeted 5-HT_{1A} receptors located in the cingulate cortex only. At 0.16 mg/kg, it also occupied other cortical regions expressing post-synaptic receptors, but it displayed weaker binding in the dorsal raphe compared to NLX-112, a result which is consistent with previous invasive studies [3].

Hemodynamic effects

Consistently with different binding patterns of NLX-112 and NLX-101, the agonists elicited different modifications of BOLD signal. Before discussing these differences in detail, some general remarks can be made. First, the effects of 5-HT_{1A}-biased agonists on BOLD signal were mixed, either excitatory or inhibitory. Despite the difficulty in interpreting negative BOLD responses in fMRI [33], it is not uncommon to observe such effects in pharmacological MRI [17]. It is also not surprising to observe mixed effects with 5-HT_{1A} ligands considering that 5-HT_{1A} receptors are expressed by a wide variety of neuronal populations, such as glutamatergic, GABAergic or cholinergic neurons for post-synaptic heteroreceptors, and serotonergic neurons for presynaptic autoreceptors [34], and can couple to multiple transduction pathways [35]. A second important remark is that BOLD responses were complex to interpret because they did not necessarily vary proportionally to agonist doses, each dose displaying a distinct functional signature, a finding that has already been observed in other pharmacological MRI studies [36]. This can be explained by the complex nature of BOLD signal, which is only indirectly related to neuronal activity [17]. Moreover, neuronal activity itself can be modified due to the direct stimulation of neuroreceptors by agonists or by indirect effects on other neurons implicated in the network. This consideration also explains why the fMRI patterns measured in our study were not necessarily spatially correlated with occupancy patterns.

In a general manner, NLX-112 induced BOLD decreases in amygdala, hippocampus and various cortical regions, with a diffuse effect at 0.04 mg/kg, weak effect at 0.08 mg/kg and maximal effect at 0.16 mg/kg. At this dose, the inhibition pattern was visually close to the PET-binding pattern at post-synaptic 5-HT_{1A} receptors. BOLD increases were found at 0.08 and 0.16 mg/kg in the frontal cortex, the dorsal raphe nucleus and the cerebellar grey matter. At the highest dose a unilateral activation was found in the temporal cortex, which might be explained by mixed effects of NLX-112 (acting at pre- and post-synaptic receptors), as the PET results show that at this dose the agonist strongly binds to receptors in the dorsal raphe nucleus. Indeed, autoreceptor stimulation can induce a decrease of serotonin release [37], which can result in variable effects on BOLD signal in projection areas [38, 39].

Hemodynamic responses induced by NLX-101 at 0.08 and 0.16 mg/kg were comparable, with a BOLD decrease in the amygdala and the hippocampus, and an increase in the frontal cortex and the cerebellum. Despite a widespread occupancy of 5-HT_{1A} receptors at 0.16 mg/kg, NLX-101 did not produce effects on BOLD signal as large as those of NLX-112. At 0.04 mg/kg, however, NLX-101 produced multiple inhibitions in cortex and some activations in the frontal cortex and the cerebellum. These findings are difficult to interpret because no occupancy was observed at this dose. It is possible that, at 0.04 mg/kg of NLX-101, binding is too limited and transitory to be quantified in PET.

The phMRI data were also analysed using a functional connectivity approach, similarly to a previous study in mice using 8-OH-DPAT [40]. This analysis provided complementary information concerning the central modifications induced by the ligands. Taken together, our results show that both NLX-112 and NLX-101 at low doses tend to increase the global functional connectivity in the cat brain compared to the control condition, but this global effect is reduced or even abolished for NLX-112 at the highest dose injected. Thus, at 0.04 mg/kg, NLX-112 produced an increase of connectivity mostly between the regions expressing high to moderate amounts of post-synaptic 5-HT_{1A} receptors, such as hippocampus and cortex. The correlation matrix for NLX-101 at the same dose was more difficult to interpret, with correlations found between cortical regions and cerebellum, excluding the temporal cortex. This result must be related to the multiple effects of NLX-101 on BOLD signal at 0.04 mg/kg, as we found both inhibitions and activations in different cortical regions and a strong activation in the cerebellum. At the intermediate dose, NLX-101 and NLX-112 produced similar correlation matrices, consistent with the similar activation maps in the voxel-based fMRI analysis. Interestingly, the correlations between the dorsal raphe nucleus and the rest of the brain were higher for NLX-112 than NLX-101, consistent with the preference of NLX-101 for post-synaptic 5-HT_{1A} receptors versus autoreceptors at this dose, that is also suggested by the voxel-based analyses of PET and fMRI data. At 0.16 mg/kg, the correlation matrix of NLX-101 was very similar

to the previous dose, consistent with its biased properties and subtle effects on the BOLD signal. On the contrary, the correlation matrix at 0.16 mg/kg of NLX-112 was completely different from the previous doses, with a global decrease of functional connectivity compared to the other conditions, which was anticipated given the mixed effects of the molecule on the BOLD signal (activations in the dorsal raphe and frontal cortex, inhibition in the cingulate and occipital cortices).

PET-MR correlation maps

A multimodal PET/MR voxel-based analysis was used to take full advantage of the PET-MR device. These correlation maps enable visualisation of voxels where BOLD increases or decreases are correlated to an increase in 5-HT_{1A} occupancy. The two maps were very different between NLX-112 and NLX-101, consistent with their different functional features. NLX-112 induced a negative BOLD effect in parallel to binding at post-synaptic 5-HT_{1A} receptors located in the amygdala, the cingulate cortex or the lateral septum. This is consistent with the inhibitory effects of 5-HT_{1A} receptors on neuronal activity, mediated mainly through adenylate cyclase inhibition and G-protein-coupled inwardly rectifying potassium channels [35]. A strong positive correlation was observed in the dorsal raphe nucleus, meaning that the stimulation of 5-HT_{1A} receptors in this region induces an increase of BOLD signal (also directly highlighted by fMRI maps). As the stimulation of autoreceptors induces a decrease of serotonergic neurons' spontaneous firing rate [37], this 'braking' of the serotonergic system may induce a local energy demand, which could explain the BOLD increase in the dorsal raphe nucleus [33]. In contrast, strong positive correlations were observed for NLX-101 in the cingulate cortex, an opposite effect to that of NLX-112. These results are consistent with the reported biased agonist properties of NLX-101 and its pro-activatory effects in cortical areas, and in favour of a possible ability to distinguish between different subpopulations of receptors in cortex [3, 41]. Indeed, 5-HT_{1A} agonists can induce a local increase or decrease of cortical neuronal activity depending on the stimulation of receptors expressed by glutamatergic or GABAergic neurons [8].

Methodological considerations

[^{18}F]MPPF was used for PET imaging as it is a well-validated 5-HT_{1A} radiotracer in animal and human [42, 43]. Similarly to previous studies using this tracer with cats [12, 13, 16], specific binding was estimated using the cerebellum as a reference region, since it is almost devoid of receptors [44]. [^{18}F]MPPF was administered as a bolus followed by constant infusion to measure changes in 5-HT_{1A} occupancy during the scans. The injection time of agonists (50 min after the bolus) was chosen to ensure a sufficient duration for the time-activity curves to reach a pseudo-equilibrium state. Four cats were used for the whole protocol (including seven experimental conditions per subject). Our protocol was designed to limit as much as possible the variability of the results, by using the same animals for the different doses of ligands, and by comparing the PET and phMRI data before and after the injection for each scan to generate the statistical maps. For each subject, scans were separated by at least 14 days and conditions were randomised to avoid confounding factors. As the fMRI signal can be influenced by changes in systemic parameters, respiratory rate, heart rate, body temperature, SpO_2 and end-tidal CO_2 were continuously monitored during acquisitions, and animals were intubated and artificially ventilated. No changes in these parameters were detected among the different conditions.

This study design has some limitations, mostly inherent to the adaptation of the protocol for repeated scans and/or future studies in human. Cats were anaesthetised with isoflurane during the scan, which is known to disrupt serotonergic neurons firing rate [45] and neuroreceptors coupling with G proteins [46]. This anaesthetic was chosen because it is suitable for a repeated use and often used in pharmacological MRI studies as it induces a stable and controllable anaesthesia [47]. Moreover, despite the limited BOLD signal changes usually measured in fMRI, we chose not to employ a contrast agent given the high number of scans performed on each animal, and so that our methodology could be directly reproduced in human subjects.

Clinical implications and conclusion

Serotonin 5-HT_{1A} receptors are attractive therapeutic targets for pharmacotherapy of various brain disorders such as anxiety, depression, schizophrenia or Parkinson's disease. The development of biased 5-HT_{1A} agonists is highly desirable to achieve selective targeting of subpopulations of 5-HT_{1A} receptors in specific brain regions, improving therapeutic effects while avoiding side-effects. For instance, the decrease of the 5-HT neurons' firing rate induced by the stimulation of 5-HT_{1A} autoreceptors in raphe nuclei may be undesirable in several neuropsychiatric indications in which the preferential stimulation of post-synaptic receptors would be beneficial, such as major depression. Here, we used simultaneous PET and fMRI to demonstrate for the first time in vivo that at the same doses, two highly specific biased agonists can target different regions, and even produce opposite effects in the same region. Importantly, our methodology is completely suitable for studies in human. Finally, these data show that simultaneous PET/fMRI is a helpful technique to non-invasively investigate the promising concept of biased agonism [48].

ACKNOWLEDGEMENTS

We thank Thomas Troalen (Siemens Healthiness France) for assistance with the PET/MR camera, Thibault Iecker and Christian Tourvielle for the production of [^{18}F]MPPF and Véronique Gualda for the zootechnical assistance.

FUNDING:

This work was supported by the Fondation NEURODIS, the IHU CESAME and the French national programme 'Investissement d'Avenir' Programmes (LILI – Lyon Integrated Life Imaging: hybrid MR-PET ANR-11-EQPX-0026), and performed within the framework of the LABEX PRIMES (ANR-11-LABX-0063) of Université de Lyon, within the programme 'Investissements d'Avenir' (ANR-11-IDEX-0007) operated by the French National Research Agency (ANR).

REFERENCES

1. Luttrell LM, Maudsley S, Bohn LM. Fulfilling the promise of "biased" G protein-coupled receptor agonism. Mol Pharmacol. 2015;88:579–88.
2. Mannoury la Cour C, El Mestikawy S, Hanoun N, Hamon M, Lanfumey L. Regional differences in the coupling of 5-hydroxytryptamine-1A receptors to G proteins in the rat brain. Mol Pharmacol. 2006;70:1013–21.
3. Newman-Tancredi A. Biased agonism at serotonin 5-HT1A receptors: preferential postsynaptic activity for improved therapy of CNS disorders. Neuropsychiatry. 2011;1:149–64.
4. Abdala AP, Bissonnette JM, Newman-Tancredi A. Pinpointing brainstem mechanisms responsible for autonomic dysfunction in Rett syndrome: therapeutic perspectives for 5-HT1A agonists. Front Physiol. 2014;5:205.
5. Iderberg H, McCreary AC, Varney MA, Kleven MS, Koek W, Bardin L, et al. NLX-112, a novel 5-HT1A receptor agonist for the treatment of L-DOPA-induced dyskinesia: behavioral and neurochemical profile in rat. Exp Neurol. 2015;271:335–50.
6. Newman-Tancredi A, Martel JC, Assié MB, Buritova J, Lauressergues E, Cosi C, et al. Signal transduction and functional selectivity of F15599, a preferential post-synaptic 5-HT1A receptor agonist. Br J Pharmacol. 2009;156:338–53.

7. Newman-Tancredi A, Martel JC, Cosi C, Heusler P, Lestienne F, Varney MA, et al. Distinctive in vitro signal transduction profile of NLX-112, a potent and efficacious serotonin 5-HT1A receptor agonist. J Pharm Pharmacol. 2017;69: 1178–90.
8. Llado-Pelfort L, Assie MB, Newman-Tancredi A, Artigas F, Celada P. In vivo electrophysiological and neurochemical effects of the selective 5-HT1A receptor agonist, F13640, at pre- and postsynaptic 5-HT1A receptors in the rat. Psychopharmacology. 2012;221:261–72.
9. Buritova J, Berrichon G, Cathala C, Colpaert F, Cussac D. Region-specific changes in 5-HT1A agonist-induced extracellular signal-regulated kinases 1/2 phosphorylation in rat brain: a quantitative ELISA study. Neuropharmacology. 2009;56:350–61.
10. Becker G, Bolbos R, Costes N, Redouté J, Newman-Tancredi A, Zimmer L. Selective serotonin 5-HT1A receptor biased agonists elicit distinct brain activation patterns: a pharmacoMRI study. Sci Rep. 2016;6:26633.
11. Carson RE. PET physiological measurements using constant infusion. Nucl Med Biol. 2000;27:657–60.
12. Aznavour N, Rbah L, Léger L, Buda C, Sastre JP, Imhof A, et al. A comparison of in vivo and in vitro neuroimaging of 5-HT 1A receptor binding sites in the cat brain. J Chem Neuroanat. 2006a;31:226–32.
13. Aznavour N, Rbah L, Riad M, Reilhac A, Costes N, Descarries L, et al. A PET imaging study of 5-HT(1A) receptors in cat brain after acute and chronic fluoxetine treatment. NeuroImage. 2006b;33:834–42.
14. Lancelot S, Costes N, Lemoine L, Zimmer L. Development and evaluation of a digital atlas for PET neuroimaging in domestic cat (Felis catus). Eur J Nucl Med Mol Imaging. 2010;37:S387–7.
15. Casanova R, Ryali S, Baer A, Laurienti PJ, Burdette JH, Hayasaka S, et al. Biological parametric mapping: a statistical toolbox for multimodality brain image analysis. NeuroImage. 2007;34:137–43.
16. Ginovart N, Hassoun W, Le Bars D, Weissmann D, Leviel V. In vivo characterization of p-[(18)F]MPPF, a fluoro analog of WAY-100635 for visualization of 5-HT(1a) receptors. Synapse. 2000;35:192–200.
17. Jenkins BG. Pharmacologic magnetic resonance imaging (phMRI): imaging drug action in the brain. NeuroImage. 2012;62:1072–85.
18. Zimmer L, Luxen A. PET radiotracers for molecular imaging in the brain: past, present and future. NeuroImage. 2012;61:363–70.
19. Hansen HD, Mandeville JB, Sander CY, Hooker JM, Catana C, Rosen BR, et al. Functional characterization of 5-HT1B receptor drugs in non-human primates using simultaneous PET-MR. J Neurosci. 2017;37:10671–8.
20. Mandeville JB, Liu CH, Vanduffel W, Marota JJ, Jenkins BG. Data collection and analysis strategies for phMRI. Neuropharmacology. 2014;84:65–78.
21. Sander CY, Hooker JM, Catana C, Normandin MD, Alpert NM, Knudsen GM, et al. Neurovascular coupling to D2/D3 dopamine receptor occupancy using simultaneous PET/functional MRI. Proc Natl Acad Sci USA. 2013;110:11169–74.
22. Sander CY, Hooker JM, Catana C, Rosen BR, Mandeville JB. Imaging agonist-induced D2/D3 receptor desensitization and internalization in vivo with PET/fMRI. Neuropsychopharmacology. 2016;41:1427–36.
23. Wey HY, Catana C, Hooker JM, Dougherty DD, Knudsen GM, Wang DJ, et al. Simultaneous fMRI-PET of the opioidergic pain system in human brain. NeuroImage. 2014;102:275–82.
24. Kumar JS, Prabhakaran J, Majo VJ, Milak MS, Hsiung SC, Tamir H, et al. Synthesis and in vivo evaluation of a novel 5-HT1A receptor agonist radioligand [O-methyl- 11C]2-(4-(4-(2-methoxyphenyl)piperazin-1-yl)butyl)-4-methyl-1,2,4-triazine-3,5(2H,4H) dione in nonhuman primates. Eur J Nucl Med Mol Imaging. 2007;34:1050–60.
25. Shrestha SS, Liow JS, Lu S, Jenko K, Gladding RL, Svenningsson P, et al. 11)C-CUMI-101, a PET radioligand, behaves as a serotonin 1A receptor antagonist and also binds to α(1) adrenoceptors in brain. J Nucl Med. 2014;55:141–6.
26. Hirani E, Opacka-Juffry J, Gunn R, Khan I, Sharp T, Hume S. Pindolol occupancy of 5-HT(1A) receptors measured in vivo using small animal positron emission tomography with carbon-11 labeled WAY 100635. Synapse. 2000;36:330–41.
27. Martinez D, Hwang D, Mawlawi O, Slifstein M, Kent J, Simpson N, et al. Differential occupancy of somatodendritic and postsynaptic 5HT(1A) receptors by pindolol: a dose-occupancy study with [11C]WAY 100635 and positron emission tomography in humans. Neuropsychopharmacology. 2001;24:209–29.
28. Maurel JL, Autin JM, Funes P, Newman-Tancredi A, Colpaert F, Vacher B. High-efficacy 5-HT1A agonists for antidepressant treatment: a renewed opportunity. J Med Chem. 2007;50:5024–33.
29. Colpaert FC, Tarayre JP, Koek W, Pauwels JP, Bardin L, Xu XJ, et al. Large-amplitude 5-HT1A receptor activation: a new mechanism of profound, central analgesia. Neuropharmacology. 2002;43:945–58.
30. McCreary AC, Varney MA, Newman-Tancredi A. The novel 5-HT1A receptor agonist, NLX-112 reduces l-DOPA-induced abnormal involuntary movements in rat: a chronic administration study with microdialysis measurements. Neuropharmacology. 2016;105:651–60.
31. Udo de Haes JI, Harada N, Elsinga PH, Maguire RP, Tsukada H. Effect of fenfluramine-induced increases in serotonin release on [18F]MPPF binding: a continuous infusion PET study in conscious monkeys. Synapse. 2006;59:18–26.
32. Zimmer L, Mauger G, Le Bars D, Bonmarchand G, Luxen A, Pujol JF. Effect of endogenous serotonin on the binding of the 5-hT1A PET ligand 18F-MPPF in the rat hippocampus: kinetic beta measurements combined with microdialysis. J Neurochem. 2002;80:278–86.
33. Lauritzen M, Mathiesen C, Schaefer K, Thomsen KJ. Neuronal inhibition and excitation, and the dichotomic control of brain hemodynamic and oxygen responses. NeuroImage. 2012;62:1040–50.
34. Santana N, Bortolozzi A, Serrats J, Mengod G, Artigas F. Expression of serotonin1A and serotonin2A receptors in pyramidal and GABAergic neurons of the rat prefrontal cortex. Cereb Cortex. 2004;14:1100–9.
35. Polter AM, Li X. 5-HT1A receptor-regulated signal transduction pathways in brain. Cell Signal. 2010;22:1406–12.
36. Steward CA, Marsden CA, Prior MJ, Morris PG, Shah YB. Methodological considerations in rat brain BOLD contrast pharmacological MRI. Psychopharmacology. 2005;180:687–704.
37. Andrade R, Huereca D, Lyons JG, Andrade EM, McGregor KM. 5-HT1A receptor-mediated autoinhibition and the control of serotonergic cell firing. ACS Chem Neurosci. 2015;6:1110–5.
38. McKie S, Del-Ben C, Elliott R, Williams S, del Vai N, Anderson I, et al. Neuronal effects of acute citalopram detected by pharmacoMRI. Psychopharmacology. 2005;180:680–6.
39. Preece MA, Taylor MJ, Raley J, Blamire A, Sharp T, Sibson NR. Evidence that increased 5-HT release evokes region-specific effects on blood-oxygenation level-dependent functional magnetic resonance imaging responses in the rat brain. Neuroscience. 2009;159:751–9.
40. Razoux F, Baltes C, Mueggler T, Seuwen A, Russig H, Mansuy I, et al. Functional MRI to assess alterations of functional networks in response to pharmacological or genetic manipulations of the serotonergic system in mice. NeuroImage. 2013;74:326–36.
41. Depoortere R, Auclair AL, Bardin L, Colpaert FC, Vacher B, Newman-Tancredi A. F15599, a preferential post-synaptic 5-HT1A receptor agonist: activity in models of cognition in comparison with reference 5-HT1A receptor agonists. Eur Neuropsychopharmacol. 2010;20:641–54.
42. Costes N, Merlet I, Ostrowsky K, Faillenot I, Lavenne F, Zimmer L, et al. A 18F-MPPF PET normative database of 5-HT1A receptor binding in men and women over aging. J Nucl Med. 2005;46:1980–9.
43. Aznavour N, Zimmer L. [18F]MPPF as a tool for the in vivo imaging of 5-HT1A receptors in animal and human brain. Neuropharmacology. 2007;52:695–707.
44. Charnay Y, Leger L, Vallet PG, Greggio B, Hof PR, Cespuglio R, et al. Mapping of 5-HT1a receptor binding sites in the feline brain: a quantitative autoradiographic study using [3H]8-OH-DPAT. Biog Amines. 1997;13:217–32.
45. Massey CA, Iceman KE, Johansen SL, Wu Y, Harris MB, Richerson GB. Isoflurane abolishes spontaneous firing of serotonin neurons and masks their pH/CO(2) chemosensitivity. J Neurophysiol. 2015;113:2879–88.
46. Seeman P, Kapur S. Anesthetics inhibit high-affinity states of dopamine D2 and other G-linked receptors. Synapse. 2003;50:35–40.
47. Haensel JX, Spain A, Martin C. A systematic review of physiological methods in rodent pharmacological MRI studies. Psychopharmacology. 2015;232:489–99.
48. Kenakin T, Christopoulos A. Signalling bias in new drug discovery: detection, quantification and therapeutic impact. Nat Rev Drug Discov. 2013;12:205–16.